

Mechanical strain induced topological phase changes of few layer ZrTe_5

Zoltán Tajkov,^{1,2} Konrád Kandrai,¹ Dániel Nagy,³

Levente Tapasztó,¹ János Koltai,⁴ and Péter Nemes-Incze¹

¹*HUN-REN Centre for Energy Research,*

Institute of Technical Physics and Materials Science, 1121 Budapest, Hungary

²*Centre of Low Temperature Physics, Institute of Experimental Physics,*

*Slovak Academy of Sciences, Košice SK-04001, Slovakia**

³*ELTE Eötvös Loránd University, Department of
Physics of Complex Systems, 1117 Budapest, Hungary*

⁴*ELTE Eötvös Loránd University, Department
of Biological Physics, 1117 Budapest, Hungary*

(Dated: November 9, 2023)

Abstract

Understanding the topological aspects of the band structure of solids has fundamentally changed our appreciation of their properties. The layered, van der Waals transition-metal pentatelluride ZrTe_5 has proven on numerous occasions to be an excellent candidate for the study of controllable topological phase transitions. Here, we investigate the topological phase diagrams of monolayer and bilayer forms of ZrTe_5 , under mechanical deformations using *ab initio* techniques. We find that mechanical deformation can close the monolayer's topological gap, while the bilayer exhibits richer phase diagram, including both topological insulating, trivial metallic and insulating phases. The bilayer is predicted to be on the topological phase boundary. We also address the preparation of monolayers, using *ab initio* simulations and experimental scanning tunneling microscopy measurements. We confirm that while monolayer ZrTe_5 is difficult to exfoliate without compromising its crystalline structure, bilayers offer a more stable alternative, revealing the complexities and limitations of using gold substrates for monolayer exfoliation.

I. INTRODUCTION

Since the seminal discovery of time-reversal invariant topological insulators, a controllable topological phase transition in two-dimensional materials remains a targeted objective in the field of solid-state physics [1–4]. Such phase transitions are characterized by changes in the topological properties of the materials band structure [5, 6]. One effective approach for accomplishing this involves tuning the lattice parameters of topological materials, potentially through mechanical deformation. The transition-metal pentatelluride, ZrTe_5 , resides at the boundary between weak and strong topological phases [4, 7–13], thus enabling the use of strain to toggle between these phases. Indeed, transitions in bulk or thick exfoliated crystal samples have been observed in prior work [3, 4, 13–16]. The material also exhibits a variety of other noteworthy phenomena. These include the planar Hall effect [17], anomalous Hall effect [18], and chiral magnetic effect [19]. For bulk samples, a Dirac semimetal-like band structure has been predicted based on early studies of quantum oscillations [20], optical conductivity [21], and photoemission [19].

Significant effort has been devoted to and still focuses on understanding the properties

* tajkov.zoltan@ek-cer.hu

of bulk ZrTe_5 . Yet, studies on few-layer to monolayer crystals are not as comprehensive, especially concerning the behavior of the ZrTe_5 system under mechanical deformations. The bulk crystal is known to be highly sensitive to minor changes in its lattice parameters. Transport measurements reveal non-monotonic strain dependence and a switch in the sign of the Dirac mass with deformation [9]. Existing ARPES measurements show that under external strain, the band gap increases with tensile strain and decreases with compressive strain [22].

Intentionally induced, controllable mechanical distortion effectively switches topological phases in the crystal. This can significantly change the electrical properties of a material, including its topological characteristics [13, 23–27]. In contrast, for thin [28, 29] to monolayer [30] samples, experimental studies of ZrTe_5 or its sister compound HfTe_5 remain scarce. Nonetheless, recent advancements have been made in the production of thin ZrTe_5 samples through bottom-up growth [31] and Al_2O_3 assisted exfoliation [30].

Theoretical studies indicate that the monolayer is a \mathbb{Z}_2 time-reversal invariant topological insulator [32]. In this work, we investigate the topological phase diagram of monolayer and bilayer ZrTe_5 crystals under mechanical distortions, employing *ab initio* techniques. We also aim to experimentally address the gap in the preparation of mono and few-layer samples by exploring the exfoliation of thin ZrTe_5 layers onto gold substrates, following established methods [13]. Exfoliation on gold is a well known technique for preparing monolayers of van der Waals (vdW) materials that possess chalcogen terminations on their surfaces [33]. Our results reveal that this method is unviable for ZrTe_5 , as the strong attraction between the first ZrTe_5 layer and the gold substrate compromises the crystalline structure of the initial layer.

II. RESULTS AND DISCUSSION

A. Topological phase diagrams of monolayer and bilayer ZrTe_5

Zirconium pentatelluride (ZrTe_5) adopts a layered orthorhombic crystal structure. Layers spanning the $x - y$ plane form trigonal prismatic ZrTe_3 lines, which are connected by zig-zag chains of Te atoms, as illustrated in Fig. 1a). The chains form two-dimensional sheets that are stacked along the z -axis, creating a layered structure. The primitive cell of bulk ZrTe_5

contains two Zr and ten Te atoms [32]. Each ZrTe_5 layer is nominally charge neutral, and the interlayer coupling is of vdW type [32]. The mono- and bilayer initial geometry was created by simply cutting one or two layers from the bulk. The initial geometry underwent full relaxation via *ab initio* calculations (see Methods section for further details). The starting point for the relaxation were the lattice constants derived from our previous X-ray diffraction measurements of the bulk sample [13]. The relaxed and experimental geometry parameters are listed in Table I. Our analysis reveals that the in-plane unit cell parameters and internal atomic coordinates closely align with their 3D bulk experimental values, corroborating previous findings [32]. The main difference between the density functional theory (DFT) codes lies in their prediction of interlayer distances in the bilayer. In particular, the SIESTA geometry relaxations yield a distance that is 0.13 Å less than that predicted by VASP. Further discussion on this discrepancy will be provided later.

		a [Å]	b [Å]	c [Å]	
Experimental	Bulk	1.994	7.265	13.724	
	SIESTA	Monolayer	1.999	N.A.	13.870
		Bilayer	1.999	7.172	13.886
VASP	Monolayer	2.002	N.A.	13.773	
	Bilayer	2.001	7.307	13.758	

TABLE I. Unit cell dimensions for ZrTe_5 as derived from the analysis of X-ray diffraction data at 300 K [13] and from relaxed DFT calculations. We note that in the few layer cases the b unit cell vector represents the interlayer distance.

It has been previously predicted that a single layer of ZrTe_5 is a \mathbb{Z}_2 time-reversal invariant topological insulator with a band gap of approximately 100 meV [32]. In Fig. 1 b)-c), we present the band structures of the unperturbed crystals, computed by both the SIESTA and VASP implementations of DFT. The blue solid lines represent the monolayer case, while the red dashed lines correspond to the bilayer. In the case of the monolayer, both SIESTA and VASP predict that the undistorted crystal is a topological insulator, albeit with slightly different band gaps: 110 meV for VASP and 70 meV for SIESTA. This consensus is broken in the bilayer scenario. VASP predicts that the bilayer is a trivial insulator with a band gap of 70 meV, whereas SIESTA anticipates a metallic phase.

As previously demonstrated, the bulk ZrTe_5 is highly sensitive to minor deformations in the crystal structure [13]. This sensitivity is also evident in the case of few-layer crystals. In Fig. 1 d)-g), we present the topological phase diagrams for mono- and bilayer ZrTe_5 under in-

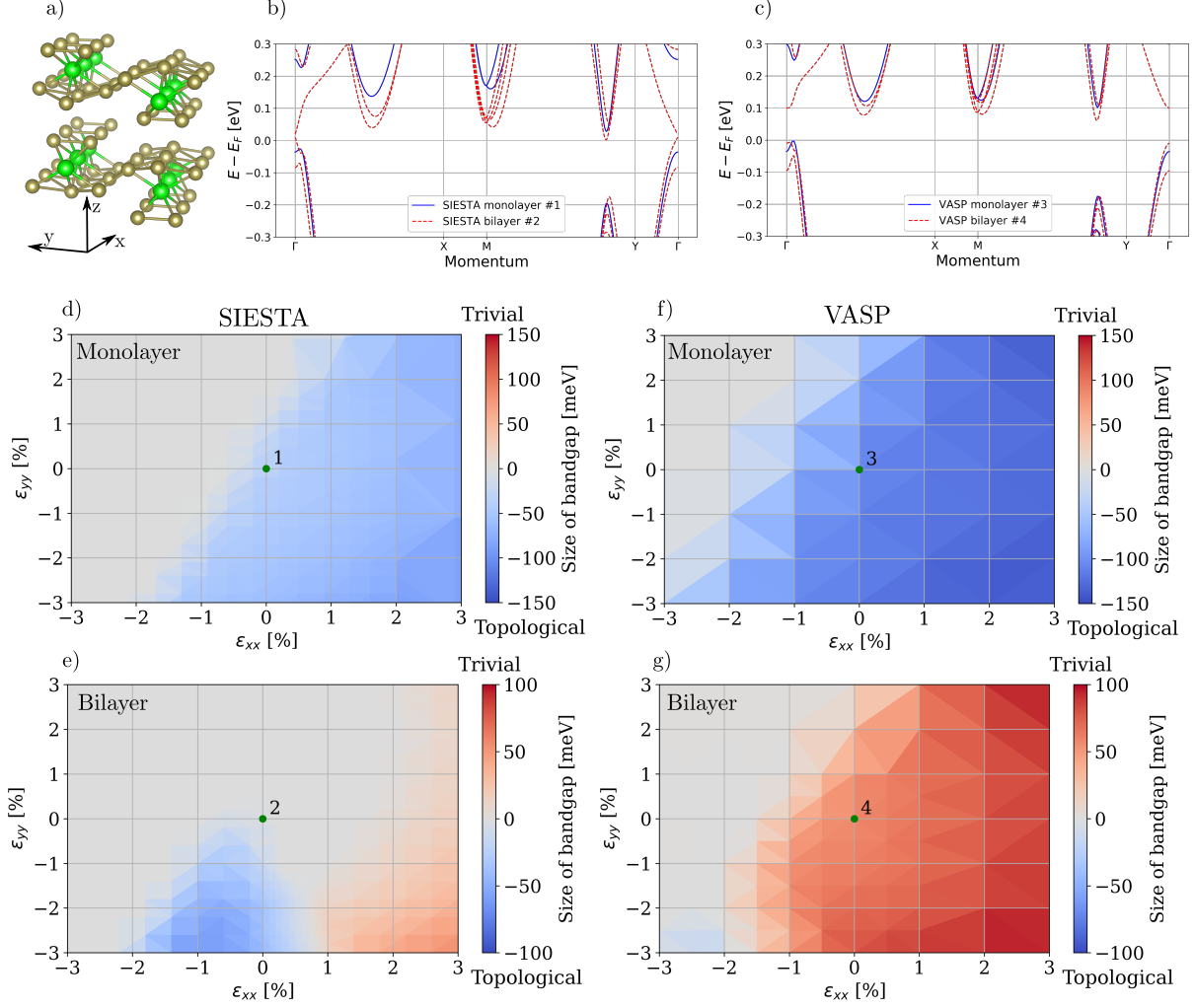


FIG. 1. **a)** The crystal structure of the bilayer. **b)** The band structures of the undistorted crystal obtained by SIESTA. The blue solid lines (dashed red) correspond to the monolayer (bilayer) case. **c)** The band structures of the undistorted crystal obtained by VASP. The blue solid lines (dashed red) correspond to the monolayer (bilayer) case. **d)-g)** The phase diagrams of the electronic structure of the crystal under mechanical strain obtained by two different DFT codes for the mono- and the bilayer cases. At every point the size of the gap was calculated and a sign has been assigned to it according to the topological favor of the gap. The negative gap corresponds to the topological insulating phase, while the positive gap to the trivial phase.

plane mechanical strain, as a function of the strain along the x and y directions: ε_{xx} and ε_{yy} . For each point on the diagram, the size of the gap is calculated, and a sign is assigned to it to indicate its topological character. A negative gap corresponds to the topological insulating phase, whereas a positive gap signifies the trivial phase. Our exploration involved analyzing the crystals using both SIESTA and VASP. As illustrated in Fig. 1 d) and f), SIESTA and

VASP concur that the monolayer resides at the boundary between topological and trivial (semimetallic) phases. Applying a modest uniaxial strain, the system can be tuned from a topological insulating to metallic phase. These data suggest that the monolayer inherits from the bulk crystal the property of residing at the boundary of a topological phase transition.

In Fig. 1 e) and f), we compare the topological phase diagrams of bilayer ZrTe_5 . SIESTA predicts that the bilayer resides at the boundary between the topological insulator and metallic phases. The diagrams indicate that applying a moderate biaxial strain can transition the system into a topological phase, while an experimentally achievable biaxial strain can induce a trivial insulating phase through the metallic regime.

The differences seen in the band structures of the bilayer are also evident when comparing the phase diagrams. In Fig. 1 f), it can be observed that, according to the VASP calculations, the bilayer resides further away from the phase boundary and is in a topologically trivial phase with a significant band gap of 70 meV. However, the central feature from SIESTA, that biaxial strain can be used to transition the system into the topological phase, is confirmed by VASP, but much larger strain is required to realize the transition.

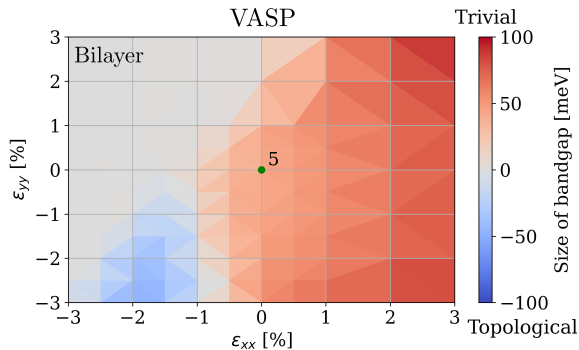


FIG. 2. The topological phase diagram of the bilayer ZrTe_5 calculated by VASP. The interlayer distance has been matched to the SIESTA optimized interlayer distance.

Further investigation into the role of geometry and lattice distortions clarifies the origin of the differences between VASP and SIESTA in the bilayer case. In Fig. 2, we present the topological phase diagrams of the bilayer calculated with VASP. This time, however, the interlayer distance has been modified to align with the SIESTA optimization results; specifically, we adjusted the distance between the layers by making it 0.13 \AA smaller. With this adjustment the predictions of the two codes converge substantially. Notably, our choice

to align VASP with SIESTA in this aspect was driven by our prior observations regarding the accuracy of SIESTA’s predictions. These observations, as discussed in Tajkov et al. (2022), revealed that SIESTA consistently yielded results that demonstrated better agreements with experimental data, particularly in the context of bulk properties of ZrTe_5 [13].

B. Exfoliation of thin ZrTe_5 onto a gold substrate

Preparing large monolayers of chalcogen terminated van der Waals materials can be easily achieved by exfoliating them onto clean gold surfaces [33]. This has been tested a wide range of dichalcogenides, including MoS_2 , WSe_2 , WS_2 , etc. and importantly for Te terminated crystals [33, 34]. For ZrTe_5 , an Al_2O_3 -based exfoliation method has been employed [30], yielding large aspect ratio monolayer flakes that have a lateral size of $\sim 10 \mu\text{m}$.

To prepare the sought after large gap 2D topological insulator phase of ZrTe_5 , we have explored the exfoliation of ZrTe_5 onto gold substrates. This method yields thick crystals, which show a good crystalline order on the top layer, as measured by scanning tunneling microscopy (STM) in our previous work [13]. The underlying principle for gold-assisted exfoliation of chalcogen-terminated materials is that the layer in direct contact with the gold forms a stronger adhesion to the gold surface than it does to the bulk crystal itself [33, 34]. This approach results in cm-sized crystals in the case of MoS_2 [34].

In our exfoliation attempts, we employ the well-known technique of evaporating gold onto a mica surface, which predominantly yields [111] facets. The gold is subsequently stripped from the mica [33], and the clean, mica-facing side is used for the exfoliation of ZrTe_5 . An optical microscopy image of such an exfoliation attempt is presented in Fig. 3a. In these experiments, the faintest optical contrast corresponds to the monolayer flakes. In our experiments, these areas are indicated by red arrows. All exfoliation experiments are conducted in a glove-box environment to minimize the risk of ZrTe_5 oxidation. We further investigate the faint monolayer areas using low-temperature (9K) STM measurements. An exemplar of these measurements is displayed in Fig. 3b. The results reveal a highly disordered structure, making it difficult to distinguish the characteristic Zr lines of ZrTe_5 . This disorder is further confirmed in the Fourier transform of the image, as shown in Fig. 3c. In contrast, STM measurements on the top layer of a multi-layer flake yield atomic resolution, and the Fourier transform of the image reveals the periodicity associated with the Zr chains, as evident in

Fig. 3d, e.

We have consistently observed the disordered nature of the monolayer candidate flakes across many tens of samples; none of these display clear atomic resolution in STM images. Given these challenges, it may be beneficial to consider alternative fabrication methods, such as the growth of monolayer ZrTe_5 via molecular beam epitaxy. In contrast, thicker flakes invariably permit atomic resolution. To shed light on this puzzling observation, we turned to *ab initio* calculations to model the interaction between ZrTe_5 and the gold [111] surface. We performed the computational study of the interface between the gold surface and multi-layer ZrTe_5 using the VASP code exclusively, as its capabilities are well-suited for such calculations. Further details can be found in the Method section. Example results of the relaxed geometry of the monolayer and the bilayer on top of a gold slab can be seen in Fig. 3f, g. These show that the monolayer becomes highly distorted on top of the gold surface.

To quantify the distortion of the ZrTe_5 layer when in contact with the gold surface, we provide histograms of the atomic distances. In Fig. 4, we display the interatomic distances in ZrTe_5 mono- and bilayers, both in gold-surface-adhered and freestanding configurations. The first row focuses specifically on the monolayer case. Panels a)-c) reveal that, in this monolayer configuration, interatomic distances undergo notable alterations, leading to a significantly deformed crystal structure compared to the freestanding case. This change is particularly prominent in the Te-Te distances, as highlighted in panel c).

Transitioning to the bilayer case, observations indicate that in this two-layer arrangement, the layer proximal to the gold surface (labelled "bottom" on Fig. 4) exhibits characteristics similar to a monolayer. Meanwhile, the top layer, aside from minor variations, largely remains intact. The most striking evidence of this phenomenon is apparent in the alterations to the Te-Te atomic distances, as seen in panel f. The relative stability of the top layer is apparent when comparing its atomic distances to those of a freestanding monolayer, as illustrated in panel g). Moreover, panel i) reveals that the interatomic distances within the gold surface also vary depending on the presence or absence of ZrTe_5 on the substrate.

Based on these findings, we conclude that exfoliating a single layer of ZrTe_5 onto a gold surface induces substantial disorder in its crystalline order. In contrast, for bilayer configurations, the layer in contact with the gold undergoes distortion while the top layer largely remains intact. It is important to mention that future research should explore how

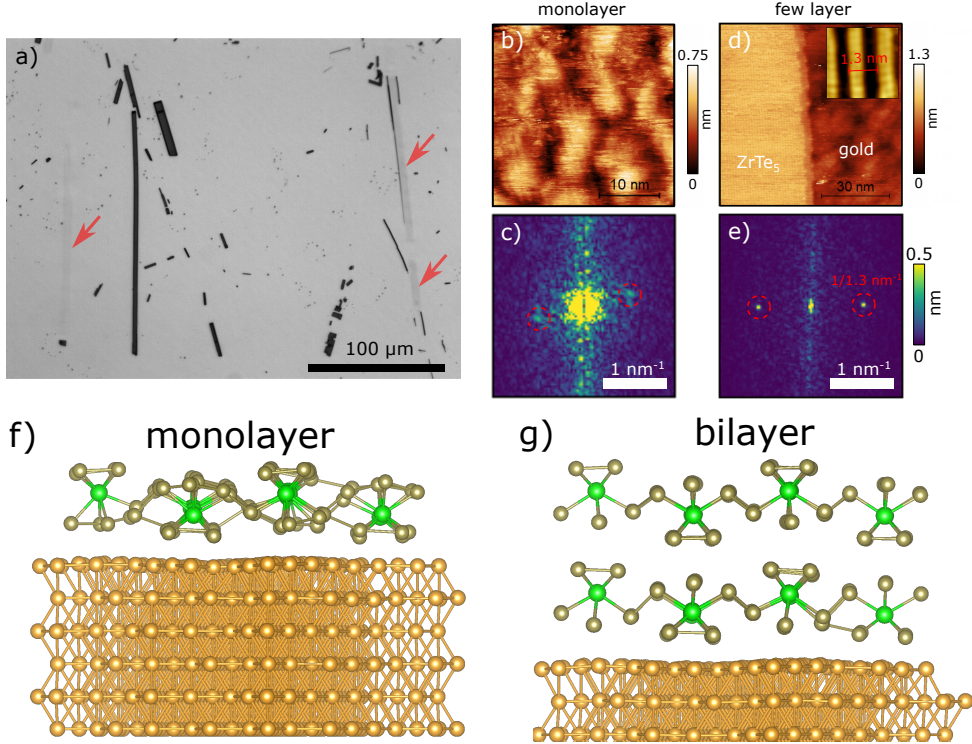


FIG. 3. **a** Optical microscopy image of exfoliated ZrTe_5 crystals on a gold surface. The thinnest crystals on the surface are marked by red arrows. **b** STM topographic image in the thinnest area, as marked by red arrows in **a**). The image shows a disordered structure. **c** Fourier transform image of the data in **b**). **d** STM topographic image of a few layer ZrTe_5 flake, showing high crystallinity, as shown by the Fourier transform in **e**). Inset: atomic resolution STM image of the surface of a thick ZrTe_5 flake, red bar marks the unit cell period in the c direction. **e** Fourier transform of the ZrTe_5 area of **d**). Red dashed circles mark the Fourier component of the periodicity in the c direction. **f-g** The relaxed geometry obtained by the VASP calculation in the monolayer and bilayer case.

closely the electrical properties of the top layer in this distorted bilayer resemble those of a freestanding monolayer.

To gain a more comprehensive understanding of the interaction between the gold surface and few-layer ZrTe_5 , we examined the bonding energies of the heterostructure. The bonding energy between the gold slab and a monolayer of ZrTe_5 is 2.43 eV per unit cell, which is more than double the bonding energy between a five-layer ZrTe_5 stack and a monolayer, recorded at 1.10 eV per unit cell. Additionally, we calculated the energy required to separate the top layer from a bilayer exfoliated onto a gold surface, finding it to be 1.16 eV per unit cell. See section IV for more details. These results indicate that while the exfoliation of monolayers is highly likely, their crystalline structure becomes compromised. This is corroborated

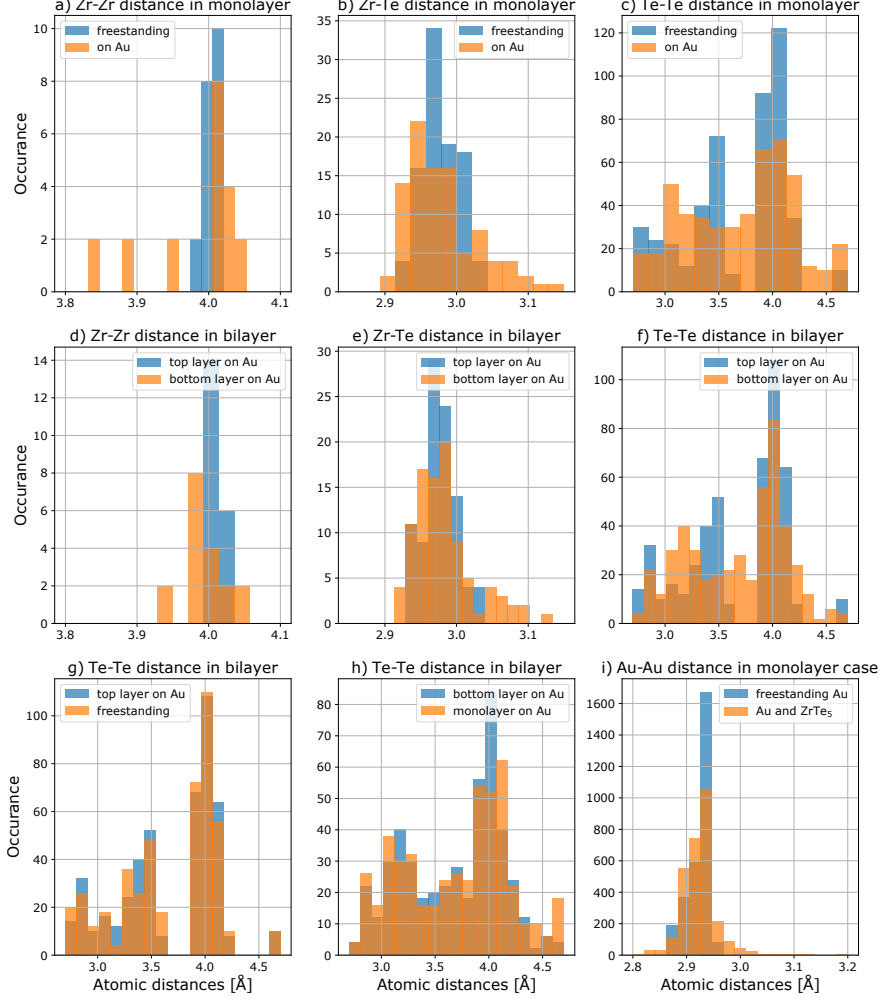


FIG. 4. Distribution of atomic distances in the few layer ZrTe_5 crystals on gold [111] surface in different configurations as calculated by the VASP code. **a-c**: Comparing the atomic distances in the ZrTe_5 monolayer for the freestanding case (blue) and relaxed on top of gold [111] (orange). **d-f** For bilayer ZrTe_5 , we compare atomic distances between the "top" layer, which is not in contact with the gold surface, and the "bottom" layer, which is in direct contact with the gold surface. **g** Comparing the Te-Te distances of the "top" layer on gold to the freestanding bilayer. **f** The Te-Te distances of a bottom layer of a bilayer on gold and that of a monolayer. **i** Showing the distortion of the Au surface itself.

by our experimental observations, which reveal expansive areas in optical microscopy with the weakest optical contrast, suggesting the presence of monolayers. However, STM measurements indicate that these areas are disordered. Moreover, bilayers are marginally more likely to form than monolayers through the exfoliation process, due to the 60 meV stronger bonding discussed above. The validation of this prediction through experimental methods is a subject of ongoing investigation.

III. CONCLUSIONS

We have probed the topological phase diagram of both single- and double-layer standalone ZrTe_5 under mechanical stress, utilizing *ab initio* methods. Our investigation unveiled that the monolayer exhibits a topological insulating phase. Under the influence of modest uni- or biaxial strain, this phase can transform into a metallic state, offering valuable flexibility in tuning its properties. Unlike the monolayer, the bilayer crystal has areas in its phase diagram where it becomes a trivial insulator. Moreover, it can be tuned into either metallic or trivial insulating phases as well. Upon closer examination, it becomes evident that when a monolayer of ZrTe_5 is exfoliated onto a gold surface, it exhibits a distinctive structure, adding complexity to the exfoliation process. This observation is supported by our experimental results.

IV. METHODS

The optimized geometry and electronic properties of the crystal were obtained by the SIESTA and VASP implementations of density functional theory (DFT) [35–40].

SIESTA

SIESTA employs norm-conserving pseudopotentials to account for the core electrons and linear combination of atomic orbitals to construct the valence states. The generalised gradient approximation of the exchange and the correlation functional was used with Perdew–Burke–Ernzerhof parametrisation [41] and the pseudopotentials optimised by Rivero *et al.* [42] with a double- ζ polarised basis set and a realspace grid defined with an equivalent energy cutoff of 350 Ry for the relaxation phase and 900 Ry for the single-point calculations. The Brillouin zone integration was sampled by a $30 \times 18 \times 1$ Monkhorst–Pack k -grid for both the relaxation and the single-point calculations [43]. The geometry optimisations were performed until the forces were smaller than 0.1 eV nm^{-1} . The choice of pseudopotentials optimised by Rivero *et al.* ensures that both the obtained geometrical structures and the electronic band properties are reliable. After the successful self consistent cycles the necessary information was obtained by the sisl tool [44]. The spin orbit coupling was taken into account in the single point calculations. In the SIESTA case we have calculated the \mathbb{Z}_2 invariant using a home made tool based on the numerical method developed by Fukui and

Hatsugai [5, 45].

VASP

The VASP code was used with projector-augmented wave pseudopotentials and the optB86b-vdW functional throughout our computation which has a non-local correlation correction that approximately accounts for dispersion interactions [46]. We have found that employing this functional gives the most accurate geometries in comparison with experiments. The plane-wave cutoff energy was set to 500 eV in all calculations. The structural optimizations were performed with $20 \times 6 \times 1$ Monkhorst-Pack set of k -points until all atomic forces fell below $3 \text{ meV}/\text{\AA}$. The band structure calculations were performed in the usual way, first the charge density was obtained in a self-consistent non-collinear calculation with a $24 \times 8 \times 1$ Monkhorst-Pack set, and in the second step the band structure was evaluated along the high-symmetry lines of the Brillouin zone.

VASP calculations of ZrTe_5 on gold

We simulated the gold (111) surface by taking 6 layers of gold and fixed the bottom 2 layers during optimization. In order to get a commensurate super cell with the ZrTe_5 we needed 7 unit cells of the crystal. The supercell unit vectors are the following: $\mathbf{A}_1 = -3\mathbf{a} + \mathbf{c}$ and $\mathbf{A}_2 = 4\mathbf{a} + \mathbf{c}$, where $\mathbf{a} = (a, 0, 0)$ and $\mathbf{c} = (0, 0, c)$. This gives a 27.192° rotation between the gold and the ZrTe_5 unit cell vectors and a slight, $< 2\%$ mismatch between the ZrTe_5 and the gold slab. Altogether the gold slab + monolayer ZrTe_5 supercell contains 312 gold atoms, 14 Zr atoms and 70 Te atoms. These calculations were performed using a single Gamma-point, which is sufficient for large unit cells like this.

STM measurements

The ZrTe_5 crystals, sourced from hqgraphene.com, were exfoliated onto gold substrates within an inert glovebox setting. These samples were then moved to the UHV STM chamber, through a vacuum shuttle. We conducted STM measurements using an RHK PanScan Freedom microscope, operating at both 300 K and 9 K in an ultra-high vacuum with a base pressure of 5×10^{-11} Torr. For the STM tips, mechanically cut Pt/Ir (90%/10%) wire was employed. A high-magnification optical microscope facilitated the precise positioning of the STM near the chosen ZrTe_5 crystals.

COMPETING INTERESTS

The authors declare no competing interests.

DATA AVAILABILITY

Any further data are available from the corresponding author upon reasonable request.

ACKNOWLEDGMENTS

The work was conducted within the framework of the Topology in Nanomaterials Lendulet project, Grant No. LP2017-9/2017, with support from the European H2020 GrapheneCore3 Project No. 881603 and the Korea-Hungary bilateral project (TT-IPARI-KR-2022-00006). Financial support from Élvonal Grant KKP 138144, NKFIH OTKA grant K132869, K134437 and TKP2021-NKTA-05 grant is also acknowledged. PNI acknowledges the support of the Janos Bolyai Research Scholarship of the Hungarian Academy of Sciences. JK acknowledges that this research was supported by the Ministry of Culture and Innovation and the National Research, Development and Innovation Office within the Quantum Information National Laboratory of Hungary (Grant No. 2022-2.1.1-NL-2022-00004). ZT acknowledges financial support from Slovak Academy of Sciences project IMPULZ IM-2021-42.

-
- [1] S. Murakami, S. Iso, Y. Avishai, M. Onoda, and N. Nagaosa, Tuning phase transition between quantum spin Hall and ordinary insulating phases, *Physical Review B* **76**, 205304 (2007).
 - [2] S. Murakami, Phase transition between the quantum spin Hall and insulator phases in 3D: emergence of a topological gapless phase, *New Journal of Physics* **9**, 356 (2007).
 - [3] J. Lu, G. Zheng, X. Zhu, W. Ning, H. Zhang, J. Yang, H. Du, K. Yang, H. Lu, Y. Zhang, *et al.*, Thickness-tuned transition of band topology in ZrTe_5 nanosheets, *Physical Review B* **95**, 125135 (2017).
 - [4] J. Mutch, W.-C. Chen, P. Went, T. Qian, I. Z. Wilson, A. Andreev, C.-C. Chen, and J.-H. Chu, Evidence for a strain-tuned topological phase transition in ZrTe_5 , *Science Advances* **5**, eaav9771 (2019).

- [5] T. Fukui and Y. Hatsugai, Quantum spin Hall effect in three dimensional materials: Lattice computation of \mathbb{Z}_2 topological invariants and its application to Bi and Sb, *Journal of the Physical Society of Japan* **76**, 053702 (2007).
- [6] J. K. Asbóth, L. Oroszlány, and A. Pályi, *A Short Course on Topological Insulators: Band Structure and Edge States in One and Two Dimensions*, 1st ed., *Lecture Notes in Physics*, Vol. 909 (Springer International Publishing, BerlinXXX, 2016).
- [7] X.-B. Li, W.-K. Huang, Y.-Y. Lv, K.-W. Zhang, C.-L. Yang, B.-B. Zhang, Y. Chen, S.-H. Yao, J. Zhou, M.-H. Lu, *et al.*, Experimental observation of topological edge states at the surface step edge of the topological insulator ZrTe₅, *Physical Review Letters* **116**, 176803 (2016).
- [8] G. Manzoni, L. Gragnaniello, G. Autès, T. Kuhn, A. Sterzi, F. Cilento, M. Zacchigna, V. Enenkel, I. Vobornik, L. Barba, *et al.*, Evidence for a strong topological insulator phase in ZrTe₅, *Physical Review Letters* **117**, 237601 (2016).
- [9] R. Wu, J.-Z. Ma, S.-M. Nie, L.-X. Zhao, X. Huang, J.-X. Yin, B.-B. Fu, P. Richard, G.-F. Chen, Z. Fang, *et al.*, Evidence for topological edge states in a large energy gap near the step edges on the surface of zrte 5, *Physical Review X* **6**, 021017 (2016).
- [10] H. Xiong, J. Sobota, S.-L. Yang, H. Soifer, A. Gauthier, M.-H. Lu, Y.-Y. Lv, S.-H. Yao, D. Lu, M. Hashimoto, *et al.*, Three-dimensional nature of the band structure of ZrTe₅ measured by high-momentum-resolution photoemission spectroscopy, *Physical Review B* **95**, 195119 (2017).
- [11] Y.-Y. Lv, B.-B. Zhang, X. Li, K.-W. Zhang, X.-B. Li, S.-H. Yao, Y. Chen, J. Zhou, S.-T. Zhang, M.-H. Lu, *et al.*, Shubnikov–de haas oscillations in bulk zrt e 5 single crystals: Evidence for a weak topological insulator, *Physical Review B* **97**, 115137 (2018).
- [12] J. I. Facio, E. Nocerino, I. C. Fulga, R. Wawrzynczak, J. Brown, G. Gu, Q. Li, M. Mansson, Y. Sassa, O. Ivashko, *et al.*, Engineering a pure dirac regime in ZrTe₅, *arXiv preprint arXiv:2206.13957* 10.48550/arXiv.2206.13957 (2022).
- [13] Z. Tajkov, D. Nagy, K. Kandrai, J. Koltai, L. Oroszlány, P. Süle, Z. E. Horváth, P. Vancsó, L. Tapasztó, and P. Nemes-Incze, Revealing the topological phase diagram of ZrTe₅ using the complex strain fields of microbubbles, *npj Computational Materials* **8**, 177 (2022).
- [14] E. Stillwell, A. Ehrlich, G. Kamm, and D. Gillespie, Effect of elastic tension on the electrical resistance of HfTe₅ and ZrTe₅, *Physical Review B* **39**, 1626 (1989).
- [15] Y. Zhang, C. Wang, L. Yu, G. Liu, A. Liang, J. Huang, S. Nie, X. Sun, Y. Zhang, B. Shen, *et al.*, Electronic evidence of temperature-induced lifshitz transition and topological nature in

- zrte5, Nature communications **8**, 1 (2017).
- [16] J. Niu, J. Wang, Z. He, C. Zhang, X. Li, T. Cai, X. Ma, S. Jia, D. Yu, and X. Wu, Electrical transport in nanothick ZrTe₅ sheets: From three to two dimensions, Physical Review B **95**, 035420 (2017).
- [17] P. Li, C. Zhang, J. Zhang, Y. Wen, and X. Zhang, Giant planar hall effect in the Dirac semimetal ZrTe₅- δ , Physical Review B **98**, 121108 (2018).
- [18] T. Liang, J. Lin, Q. Gibson, S. Kushwaha, M. Liu, W. Wang, H. Xiong, J. A. Sobota, M. Hashimoto, P. S. Kirchmann, *et al.*, Anomalous hall effect in ZrTe₅, Nature Physics **14**, 451 (2018).
- [19] Q. Li, D. E. Kharzeev, C. Zhang, Y. Huang, I. Pletikosić, A. Fedorov, R. Zhong, J. Schneeloch, G. Gu, and T. Valla, Chiral magnetic effect in ZrTe₅, Nature Physics **12**, 550 (2016).
- [20] Y. Liu, X. Yuan, C. Zhang, Z. Jin, A. Narayan, C. Luo, Z. Chen, L. Yang, J. Zou, X. Wu, *et al.*, Zeeman splitting and dynamical mass generation in dirac semimetal ZrTe₅, Nature Communications **7**, 1 (2016).
- [21] R. Chen, S. Zhang, J. Schneeloch, C. Zhang, Q. Li, G. Gu, and N. Wang, Optical spectroscopy study of the three-dimensional Dirac semimetal ZrTe₅, Physical Review B **92**, 075107 (2015).
- [22] P. Zhang, R. Noguchi, K. Kuroda, C. Lin, K. Kawaguchi, K. Yaji, A. Harasawa, M. Lippmaa, S. Nie, H. Weng, *et al.*, Observation and control of the weak topological insulator state in zrte5, Nature communications **12**, 1 (2021).
- [23] H. Xiang, B. Xu, J. Liu, Y. Xia, H. Lu, J. Yin, and Z. Liu, Quantum spin Hall insulator phase in monolayer WTe₂ by uniaxial strain, AIP Advances **6**, 095005 (2016).
- [24] B. Monserrat and A. Narayan, Unraveling the topology of ZrTe₅ by changing temperature, Physical Review Research **1**, 033181 (2019).
- [25] Z. Tajkov, D. Visontai, L. Oroszlány, and J. Koltai, Uniaxial strain induced topological phase transition in bismuth–tellurohalide–graphene heterostructures, Nanoscale **11**, 12704 (2019).
- [26] Z. Tajkov, J. Koltai, J. Cserti, and L. Oroszlány, Competition of topological and topologically trivial phases in patterned graphene based heterostructures, Physical Review B **101**, 235146 (2020).
- [27] C. Zhang, H. Pi, L. Zhou, S. Li, J. Zhou, A. Du, and H. Weng, Switchable topological phase transition and nonlinear optical properties in a ReC₂H monolayer, Physical Review B **105**, 245108 (2022).

- [28] F. Tang, P. Wang, M. He, M. Isobe, G. Gu, Q. Li, L. Zhang, and J. H. Smet, Two-dimensional quantum Hall effect and zero energy state in few-layer ZrTe_5 , *Nano letters* **21**, 5998 (2021).
- [29] C. Belke, S. Locmelis, L. Thole, H. Schmidt, P. Behrens, and R. J. Haug, Thickness-dependent gap energies in thin layers of hft_5 , *2D Mater.* **8**, 035029 (2021).
- [30] W. Z. Zhuo, B. Lei, C. S. Zhu, Z. L. Sun, J. H. Cui, W. X. Wang, Z. Y. Wang, T. Wu, J. J. Ying, Z. J. Xiang, and X. H. Chen, Thickness-dependent electronic structure in layered ZrTe_5 down to the two-dimensional limit, *Phys. Rev. B* **106**, 085428 (2022).
- [31] J. Wang, J. Niu, X. Li, X. Ma, Y. Yao, and X. Wu, Facile and fast growth of high mobility nanoribbons of ZrTe_5 , *Chinese Physics B* **29**, 068102 (2020).
- [32] H. Weng, X. Dai, and Z. Fang, Transition-metal Pentatelluride ZrTe_5 and HfTe_5 : A paradigm for large-gap quantum spin Hall insulators, *Physical Review X* **4**, 011002 (2014).
- [33] G. Z. Magda, J. Petó, G. Dobrik, C. Hwang, L. P. Biró, and L. Tapasztó, Exfoliation of large-area transition metal chalcogenide single layers, *Scientific Reports* **5**, 14714 (2015).
- [34] G. E. Velicky M, Donnelly, W. R. Hendren, S. McFarland, D. Scullion, W. J. I. DeBenedetti, G. C. Correa, Y. Han, A. J. Wain, M. A. Hines, D. A. Muller, K. S. Novoselov, H. D. Abruna, R. M. Bowman, E. J. G. Santos, and F. Huang, Mechanism of Gold-Assisted exfoliation of Centimeter-Sized Transition-Metal dichalcogenide monolayers, *ACS Nano* **12**, 10463 (2018).
- [35] E. Artacho, E. Anglada, O. Diéguez, J. D. Gale, A. García, J. Junquera, R. M. Martin, P. Ordejón, J. M. Pruneda, D. Sánchez-Portal, *et al.*, The SIESTA method; developments and applicability, *Journal of Physics: Condensed Matter* **20**, 064208 (2008).
- [36] J. M. Soler, E. Artacho, J. D. Gale, A. García, J. Junquera, P. Ordejón, and D. Sánchez-Portal, The SIESTA method for ab initio order-N materials simulation, *Journal of Physics: Condensed Matter* **14**, 2745 (2002).
- [37] A. García, N. Papior, A. Akhtar, E. Artacho, V. Blum, E. Bosoni, P. Brandimarte, M. Brandbyge, J. I. Cerdá, F. Corsetti, *et al.*, Siesta: Recent developments and applications, *The Journal of chemical physics* **152**, 204108 (2020).
- [38] L. Fernández-Seivane, M. A. Oliveira, S. Sanvito, and J. Ferrer, On-site approximation for spin-orbit coupling in linear combination of atomic orbitals density functional methods, *Journal of Physics: Condensed Matter* **18**, 7999 (2006).
- [39] G. Kresse and J. Hafner, *Ab initio* molecular dynamics for liquid metals, *Physical Review B* **47**, 558 (1993).

- [40] G. Kresse and J. Furthmüller, Efficient iterative schemes for *ab initio* total-energy calculations using a plane-wave basis set, *Physical Review B* **54**, 11169 (1996).
- [41] J. P. Perdew, K. Burke, and M. Ernzerhof, Generalized gradient approximation made simple, *Physical Review Letters* **77**, 3865 (1996).
- [42] P. Rivero, V. M. García-Suárez, D. Pereñíguez, K. Utt, Y. Yang, L. Bellaiche, K. Park, J. Ferrer, and S. Barraza-Lopez, Systematic pseudopotentials from reference eigenvalue sets for DFT calculations, *Computational Materials Science* **98**, 372 (2015).
- [43] H. J. Monkhorst and J. D. Pack, Special points for Brillouin-zone integrations, *Physical Review B* **13**, 5188 (1976).
- [44] N. Papior, `sisl: v0.11.0` (2021).
- [45] D. Nagy, `get_z2` (2021).
- [46] J. Klimeš, D. R. Bowler, and A. Michaelides, Van der Waals density functionals applied to solids, *Physical Review B* **83**, 195131 (2011).